Applied Physics Letters

RESEARCH ARTICLE | SEPTEMBER 04 2026

Rapidly resolving bilayer stacking orientation in industrially compatible MOCVD-grown MoS_2 films through second harmonic generation imaging

Reynolds Dziobek-Garrett ; Vina Faramarzi ; Pawan Kumar ; Vasco Tenner ; Marko Kamp ; A. Femius Koenderink ; Jorik van de Groep ; Roland Bliem

Appl. Phys. Lett. 129, 092105 (2026)
https://doi.org/10.1063/5.0334162

AIP Publishing

Applied Physics Letters ARTICLE pubs.aip.org/aip/apl

Rapidly resolving bilayer stacking orientation in industrially compatible MOCVD-grown MoS_2 films through second harmonic generation imaging

Cite as: Appl. Phys. Lett. **129**, 092105 (2026); doi: 10.1063/5.0334162
Submitted: 17 March 2026 · Accepted: 10 July 2026 ·
Published Online: 4 September 2026

Reynolds Dziobek-Garrett,[1,2,a)] Vina Faramarzi,[3] Pawan Kumar,[4] Vasco Tenner,[3] Marko Kamp,[5] A. Femius Koenderink,[5] Jorik van de Groep,[2] and Roland Bliem[1,2]

AFFILIATIONS

[1]Advanced Research Center for Nanolithography (ARCNL), Science Park 106, 1098 XG Amsterdam, The Netherlands
[2]Van der Waals-Zeeman Institute, Institute of Physics, University of Amsterdam, 1098 XH Amsterdam, The Netherlands
[3]ASML Netherlands B.V., De Run 6501, 5504 DR Veldhoven, The Netherlands
[4]IMEC, Kapeldreef 75, B-3001 Leuven, Belgium
[5]Department of Information in Matter and Center for Nanophotonics, AMOLF, Science Park 104, 1098 XG Amsterdam, The Netherlands

[a)]Author to whom correspondence should be addressed: r.dziobekgarrett@arcnl.nl

ABSTRACT

Atomically thin semiconductor films grown by metal organic chemical vapor deposition (MOCVD) will be crucial for the integration of two-dimensional (2D) materials into semiconductor devices produced at scale. However, the development of wafer-scale growth techniques has outpaced the development of corresponding metrology to assess film quality of 2D transition metal dichalcogenide (TMD) films. One particularly difficult issue is that the stacking sequence when overgrowing TMD films is not uniquely defined, with different possible orientations for the second layer. Determining this stacking order of individual grains when growing additional layers over a closed monolayer is an outstanding challenge for such films. Here, we use second harmonic generation (SHG) microscopy to assess the size, dispersion, and stacking orientation of bilayer grains in MOCVD-grown MoS_2 films. We correlate several microscopy techniques—bright-field white-light microscopy imaging, atomic force microscopy, photoluminescence mapping, and SHG microscopy—to show that SHG can uniquely map the stacking orientation of bilayer nucleates in these films. We expect this to drive the development of further metrology based on SHG for semiconductor applications, especially in the development of 2D material specific tools.

Two-dimensional (2D) transition metal dichalcogenide (TMD) semiconductors are actively being explored for high-performance transistors and other next-generation optoelectronic and photonic devices.[1] While initial proof-of-principle studies were performed on single exfoliated flakes, scalable production has required a shift toward device prototypes based on few-layer films produced through deposition techniques such as atomic layer deposition (ALD), chemical vapor deposition (CVD), and metal organic CVD (MOCVD).[2–5] These deposition techniques have rapidly progressed, including recent demonstrations of control over crystal morphology,[6,7] dopants,[8,9] and wafer-scale growth of high-quality single crystal monolayer films.[10–14] However, inspection, characterization, and metrology techniques that can rapidly assess crystal quality over large areas have not developed at the same rate.[2,15,16] Critically, simply scaling existing lab techniques used for initial prototype materials and structures such as white-light microscopy, atomic force microscopy (AFM), photoluminescence (PL) imaging, and Raman mapping have thus far been insufficient for wafer-scale TMD film metrology.

Among the lab-scale optical techniques used for routine characterization of TMDs, second harmonic generation (SHG) microscopy can map the layer number, crystal orientation, and strain of exfoliated crystals.[17–21] It has also been extensively applied to TMD films with

large grains as a probe of layer number, grain orientation, and grain boundary density.[22–24] However, it has thus far not been applied to TMD films grown by MOCVD, which is the method most compatible with material quality and fabrication requirements of advanced CMOS semiconductor devices with 2D TMD channels.[4,8,25] The application of SHG microscopy to mono- and few-layer films grown by MOCVD is crucial for motivating its further development in industrial metrology. Unfortunately, the small grains usually present in these films pose challenges for the resolution of optical techniques as they are on the same scale as the optical diffraction limit, at most a few micrometers;[5] however, recent advances in synthesis can produce much larger grain sizes through control over precursor mobility,[26] nucleation,[27] and grain orientation.[28,29] The use of epitaxial approaches, where the nucleating monolayer adopts a preferred orientation with respect to a crystalline substrate, is among the most promising approaches to achieve grain boundary free monolayer films.[5,10] However, a second layer growing on the first may not adopt the same orientation, because the van der Waals interlayer interaction of layered materials typically allows different stacking sequences. Not only can stacking arrangements lead to grain boundaries detrimental to carrier transport, but also phase purity in TMD films is desirable for specific applications such as nonlinear optics,[30] ferroelectrics,[31] or high-performance electronics.[32] Therefore, a facile assessment technique of such bilayers over large areas would be immensely useful in understanding such growth mechanisms.

Here, we show that SHG imaging can identify the size, distribution, and stacking orientation of bilayer nucleates in MOCVD-grown MoS_2 films. We study films both on their native growth substrates (sapphire) as well as films transferred to fresh sapphire substrates. Through correlative imaging, we robustly identify bilayer nucleates that are identical in optical and AFM imaging and subtly different in PL spectroscopy and mapping, but give opposite responses and high contrast in SHG images. We expect this demonstration to spur the further development of higher resolution and polarization-resolved SHG microscopy to identify other features in such industrially relevant TMD films, such as grain boundary orientation, defectivity, and strain. In turn, our results will drive the development of metrology tools for HVM of TMD-based semiconductor devices, which is currently a bottleneck for the assessment of material and device quality over wafer scales.

SHG is a nonlinear optical response characterized by a second order nonlinear susceptibility, intrinsic to the electronic and crystal structure of a material [Fig. 1(a)]. The key requirement for a nonzero SH response is the lack of inversion symmetry, which will cancel any SHG by oppositely radiating dipoles. Bulk 2H MoS_2 has inversion symmetry, as the unit cell includes two trigonal prismatic MoS_2 units oriented antiparallel to each other, known as AA′ stacking [Fig. 1(b)]. This stacking configuration is the most thermodynamically stable; however, a rhombohedral, ABC stacking order, labeled 3R, is also thermodynamically stable and can be readily grown and observed.[33] In the 3R case, adjacent layers are laterally offset [Fig. 1(c)], lifting the inversion symmetry and subtly modifying the band structure.[34] Although the full ABC stacking arrangement for 3R MoS_2 is not possible for bilayer crystals, we retain the 3R label for AB/AC stacked bilayers for consistency with literature. These two stacking arrangements, AA′ (2H) and AB/AC (3R), are thus the commonly found products of bilayers nucleating on a monolayer film.[35]

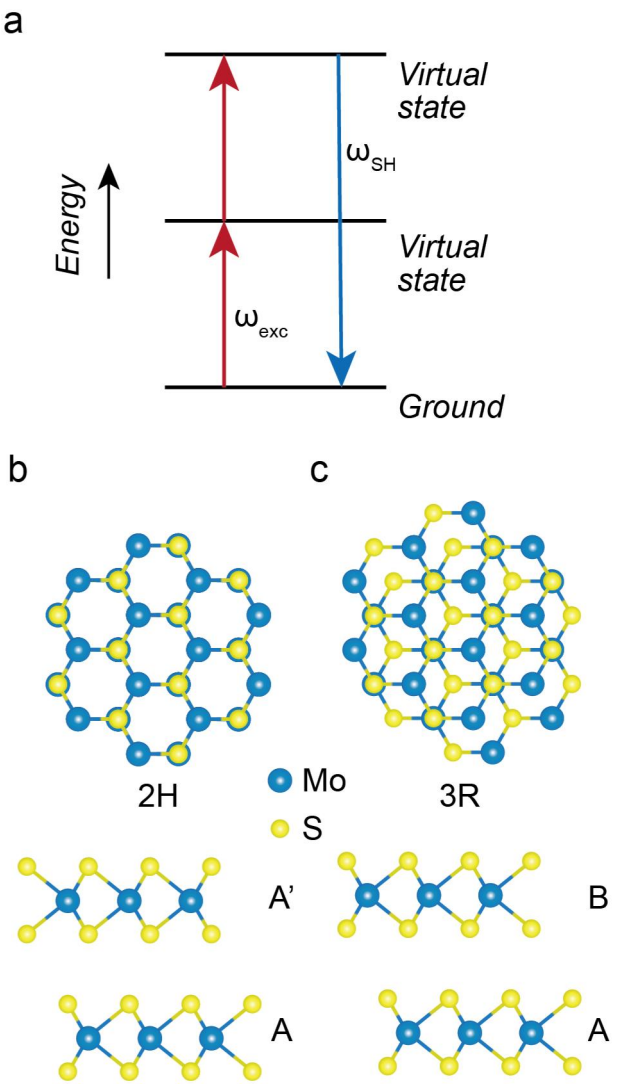

FIG. 1. (a) Energy level diagram of second harmonic generation. (b) Stacking arrangement of 2H phase bilayer MoS_2 visualized along the c axis (top) and a axis (bottom). (c) Stacking arrangement of 3R phase bilayer MoS_2 visualized along the c axis (top) and a axis (bottom).

While SHG imaging has proven an effective method for characterizing stacking order and layer number in exfoliated and CVD-grown films with large grain sizes,[17–20,22] it has yet to be demonstrated for MOCVD-grown films with smaller grains.[18,36] To test whether SHG imaging is useful for such samples, we imaged MOCVD-deposited films of MoS_2 on sapphire using a multiphoton microscope. Our SHG imaging setup is based on an inverted confocal microscope, with a tunable Ti:Sapphire laser focused with a 0.75 NA, 20× magnification objective onto the sample. The second harmonic signal is collected in reflection and passed to a photomultiplier tube detector. For our experiments, we use a fundamental wavelength of 900 nm and detect the second harmonic at 450 nm, filtering off the fundamental with a series of bandpass filters. The laser power at the sample is set to

between 2 and 8 mW at a repetition rate of 80 MHz; we observe no optically visible sample damage in that range. For further experimental details, see the supplementary material.

We rapidly scan large areas of our substrate with laser scanning, easily mapping the SH intensity response over hundreds of micrometers with acquisition times of ~1 ms μm^{-2}. The wide-field images show a highly speckled response, but zooming in reveals small, micron sized islands of dark and bright patches surrounded by a uniform background [Figs. 2(a) and 2(b)]. We assign the uniform response to SHG from the monolayer film, which we know from optical imaging fully covers the substrate [Fig. 2(c)]. We note that the closed monolayer adopts a single crystal orientation with <1% inversion domains,[28] and that such inverted grains, if present, should give the same SHG intensity with only the diminished intensity at the boundary.[22] We do not see other grain boundaries, such as those seen in SHG imaging of polycrystalline films deposited by solid-source CVD.[37] Comparison of the intensity from the dark islands with the signal from the substrate shows that these are not holes in the film [Figs. 2(d) and 2(e)], but rather islands of reduced SH intensity. Plotting the average intensity of dark islands, bright islands, monolayer, and substrate regions also reveals the significant difference of SH intensity between the dark islands and substrate regions; the dark islands are on average nearly twice as intense as the background signal from the bare substrate [Figs. 2(e) and 2(f)]. While one may hypothesize that dark islands we see in the SHG map correspond to the bright islands seen in the white-light optical images [Fig. 2(c)], we note several key differences that rule out this possibility. First, these brighter islands in the BF optical images likely correspond to trilayer or thicker islands, as supported by further AFM imaging discussed later. Second, these optically bright features are larger than the surrounding ones, whereas the dark islands in the SHG map are on average smaller than the bright islands there. Finally, the symmetry of the trilayer in either 2H or 3R stacking would lack inversion symmetry and appear bright in the SHG map, ultimately ruling out this possibility.

Coupled with the knowledge about stacking order dependence of SHG in MoS_2 crystals, we assign these dark islands to 2H (AA′) stacked bilayers; it follows that the bright islands logically must be 3R (AB/AC) stacked bilayers. Further support for our assignments comes from comparing the SHG intensity we observe for the bright islands and the monolayer regions. Subtracting the background signal from the substrate yields average intensities of 1088.2±55.9 and 2218.8±354.9 counts for monolayer and 3R bilayer regions, respectively [Fig. 2(f)]. This is a nearly perfect match with the expected intensity ratio of 2:1 for 3R bilayer vs monolayer. We can then use this information, along with image analysis, to quantify the size and distribution of bilayer islands across the films (see the supplementary material for further details). We do this for one 80 × 80 μm^2 image to show typical results. As is qualitatively apparent, quantitative analysis of bilayer islands reveals that 3R bilayers are on average more prevalent and larger than 2H islands. In fact, the 3R bilayers account for

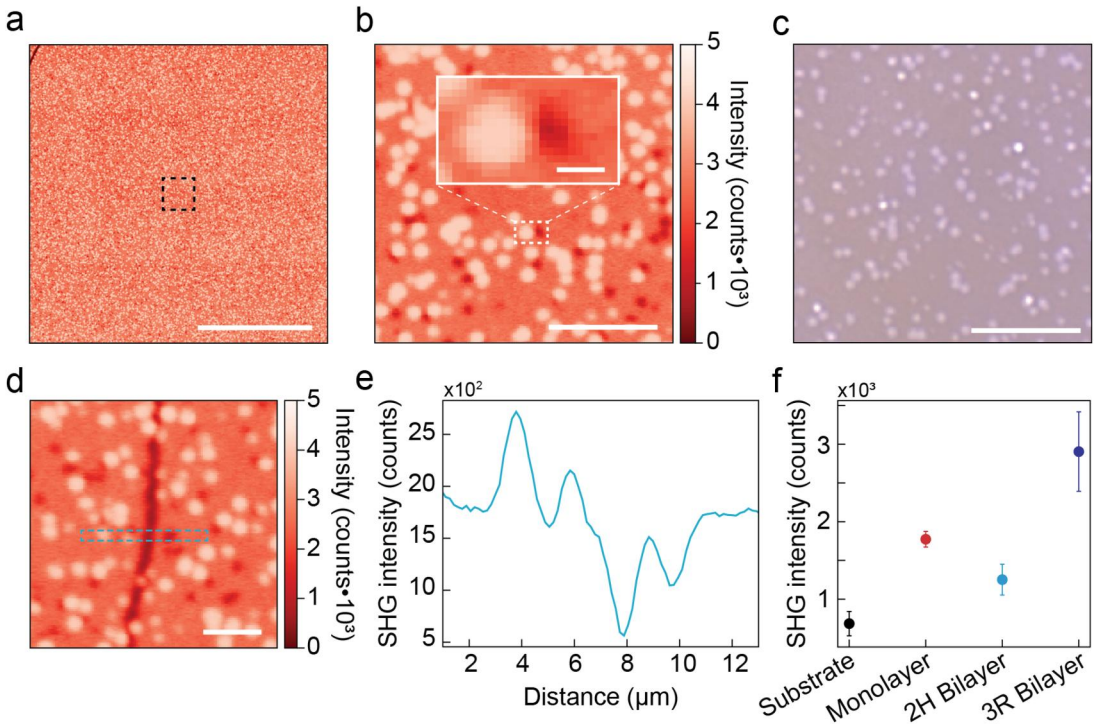

FIG. 2. (a) Large field of view SHG intensity map of an MoS_2 monolayer film and bilayer islands grown by metal organic chemical vapor deposition (MOCVD) on sapphire and transferred to a fresh sapphire surface. Scalebar: 100 μm. (b) Magnified SHG intensity map of the region outlined with the dashed box in (a). Scalebar: 10 μm. Inset: magnified SHG image of two bilayer islands with opposite intensity contrasts with the monolayer. Scalebar: 1 μm. (c) Optical image of the film. Scalebar: 10 μm. (d) SHG intensity map of a scratch in the film. Scalebar: 5 μm. (e) Intensity profile along the dashed line in (d) showing the SHG intensity of monolayer, 2H bilayer, substrate, and 3R bilayers. (f) Average SH intensity from the map in (d) for substrate, monolayer, and bilayers.

more than 65% of the bilayers (Fig. S2). Although our size estimation indicates that 3R bilayers are on average more than twice as large as their 2H counterparts, the size assessment of 2H bilayers requires further study, as the noise inherent with these dark islands and their size near the diffraction limit of the SHG measurement, coupled with particular image thresholding, may lead to an underestimation of their size. Comparison with AFM measurements of lateral size does not support the same conclusion that 2H and 3R bilayers differ greatly in size. Furthermore, we note that any grains over $\sim 15\ \mu m^2$ are almost certainly the result of coalesced grains, which are prevalent for the 3R bilayers. This leads to an overestimate of their average size but, conversely, a net underestimate of their number. We also note that TEM imaging does show the presence of some merged 2H/3R bilayer domains, which would cause further uncertainty in the size statistics.[35]

We next confirm our assignments of bilayer stacking by correlating our SHG imaging with bright-field, white-light imaging, atomic force microscopy (AFM), and photoluminescence (PL) mapping. To do this, we intentionally scratch the film to create markers, then image the areas around these scratches using all four techniques (Fig. S3). We find a region for which the SHG image shows both types of islands and substrate for proper background subtraction for PL and Raman spectroscopy. First, we examine the optical image and confirm the correlation between the two images. We clearly identify the same constellation of bilayers in both SHG and OM images, and the optical contrast is nearly uniform for all bilayer types [Figs. 3(a) and 3(c)]. We particularly focus on a cluster of three adjacent 2H bilayers and three 3R bilayers, circling one in light blue as our representative 2H island and a second, circled in dark blue, as the 3R bilayer. Although linescans of the SHG intensity show clear contrast between the two stacking configurations, their difference in optical contrast is just two percent at their respective maxima [Fig. 3(d)]. This difference is well within the range of experimental error, as the absolute difference is within 1.5σ of the optical contrast of the background, defined by a linescan along the scratch.

Second, we examine the AFM image, which shows several bilayer islands atop the monolayer. As measured by the linescans, the 3R and 2H bilayers have heights above the monolayer of 1.0 ± 0.1 and 0.9 ± 0.1 nm, respectively, consistent with the literature for measurements of a single MoS_2 layer. We also plot linescans of other bilayers with analogous results (Fig. S4). In the region of our AFM scan, we also clearly resolve a small trilayer region, which clearly corresponds to an increase in optical contrast, as well as the expected increase in SHG intensity (Fig. S5). This confirms our assertion that the few brighter optical features we observe in the wide-field optical image indeed correspond to trilayers nucleating on top of bilayers.

Finally, we turn to PL spectroscopy and mapping. We took hyperspectral PL data over our region of interest, fitting spectra to assign contributions from the A exciton (X_A), B exciton (X_B), and indirect bandgap emission (I), which arises in bilayers (Fig. S6; see the supplementary material for further details). By integrating over the fitted X_A peak we generate a PL intensity map [Fig. 4(a); for further experimental details see supplementary material]. As expected, the X_A PL intensity map clearly shows decreased PL intensity for bilayer

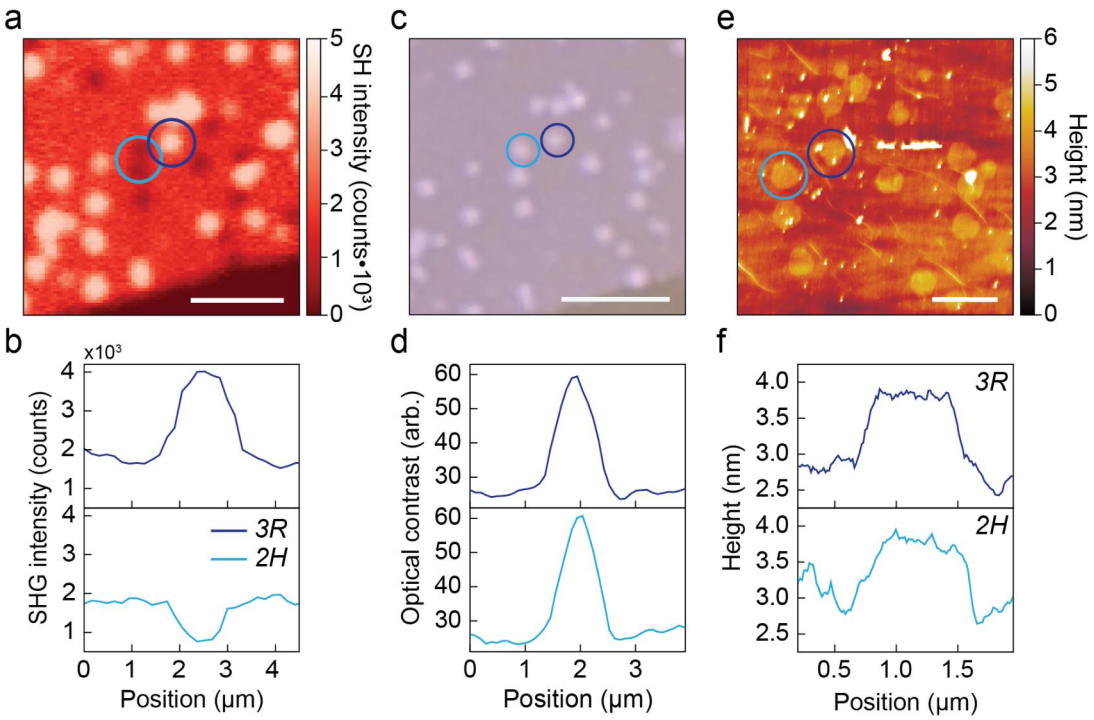

FIG. 3. (a) SHG map of an MoS_2 film transferred to a fresh sapphire surface. Scalebar: 5 μm. (b) SH intensity traces of the bilayers circled in (a). (c) Optical image of the same region as (a). Scalebar: 5 μm. (d) Optical contrast traces of the bilayers circled in (c). (e) Atomic force microscopy (AFM) image of the same area as (a). Scalebar: 2 μm. (f) AFM linescans from circled areas in (e) showing the uniform heights of bilayer islands on the monolayer film.

regions due to the indirect bandgap of bilayers and bulk; however, 2H and 3R bilayers are indistinguishable in the X_A intensity map.

We note that although the PL intensity of the bilayers is reduced compared to the monolayer, the X_A peak does not shift in energy, and the overall reduction in intensity is lower than that shown in exfoliated MoS_2 bilayers. We conducted SHG microscopy of MoS_2 mono- and bilayers exfoliated from bulk 2H MoS_2 on sapphire substrates at the same measurement power and interestingly observed a difference between the SHG intensity we observe between MOCVD-grown 2H bilayers and the exfoliated bilayers. Notably, in the exfoliated case, the 2H bilayers are nearly indistinguishable from the signal from the substrate, whereas for the MOCVD-grown bilayers, their SHG intensity is almost double that of the substrate [Fig. 4(b) and Fig. S7]. One explanation for this observation is that the degree of interlayer coupling in the MOCVD-grown 2H bilayers may be lower than that of exfoliated crystals, which leads to a subtle lifting of the inversion symmetry and thus a stronger SHG response. Concomitantly, this can lead to lower electronic coupling and thus a less significant shift toward an indirect bandgap as expected for pristine MoS_2. A simpler explanation could also be an effect of polymer residue from the transfer process from the growth substrate for the MOCVD-grown films; however, this would be expected to give a similar increase in the SHG intensity for monolayers, for which we observe nearly identical SHG intensity between MOCVD-grown and exfoliated MoS_2.

Closer inspection of PL spectra from monolayer, 3R bilayer, and 2H bilayer regions shows some notable differences. First, the PL spectra from the monolayer have a X_A peak centered at 1.84 eV with strong intensity relative to emission from defects in the sapphire substrate (Fig. S6), a linewidth of 120 meV, and a shoulder at 2.03 eV from X_B as expected for monolayer MoS_2. Comparison to spectra from bilayers shows a diminished X_A intensity and a new peak appearing around 1.5 eV which arises due to the transition to an indirect bandgap in multilayer MoS_2 which we label I_{2H} and I_{3R} [Fig. 4(c)].[34] Clearly, the position of this indirect bandgap is different for different stacking orientations; the 2H bilayers have a slightly narrower indirect gap than 3R, as indicated by a difference between I_{2H} and I_{3R} of ~26 meV. Similarly, although the X_A position is the same between monolayer, 2H, and 3R bilayers, X_B redshifts for the 3R bilayers compared to monolayer and 2H bilayers by ~13 meV. Both of these observations have been independently verified in the literature for exfoliated crystals,[20,38] MOCVD-grown bilayers,[26] and in density functional theory (DFT) calculations.[39] This discrepancy in the indirect gap energy arises due to the slightly more favorable interlayer hybridization in 2H bilayers, which leads to a slightly lower indirect bandgap between the conduction band minimum between the K and Γ points and the valence band maximum at the Γ point.[40,41] This slight decrease in coupling strength between layers in the 3R phase can also be seen in breathing modes observed in low-frequency Raman spectroscopy;[42] however, Raman mapping requires even longer integration times than PL, so we do not compare it to our SHG imaging here.

These differences in PL response between bilayers suggest that PL mapping of X_B and $I_{2H/3R}$ may also be able to distinguish between

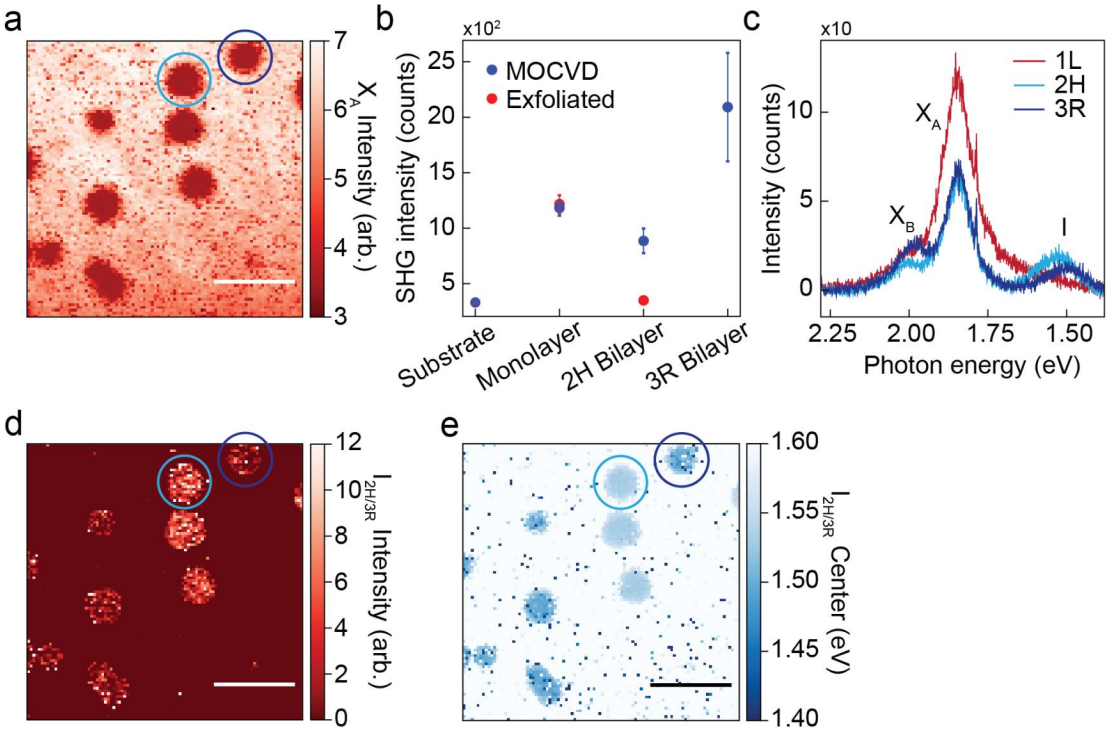

FIG. 4. (a) Photoluminescence (PL) intensity map of A exciton emission from the same area imaged in Fig. 3. (b) Scatter plot of average intensities from SHG maps in Fig. S7 from regions with bare sapphire substrate, monolayer, 2H bilayer, and 3R bilayer, which is only observed in the case of MOCVD-grown films. (c) PL spectra from circled regions in (a) showing the emission of monolayer and bilayer MoS_2. (d) Intensity map of the fitted indirect bandgap emission. (e) Map of the indirect emission peak center. Scalebars: 2 μm.

stacking orientations. To observe this, we map the integrated intensity of X_B and I, generating two additional intensity maps [Fig. 4(d) and Fig. S8]. Compared to the X_A intensity map, the X_B intensity map less clearly distinguishes between bilayer and monolayer, largely due to inhomogeneity in the fitted X_B intensity for monolayer. On the contrary, the I intensity map much more clearly resolves bilayers from the monolayer; this is expected given the qualitative difference in peak structure seen in the spectra. Furthermore, the I intensity map shows significant contrast between 2H and 3R bilayers. Comparing fitted I intensity between circled bilayers and monolayer reveals differences of 114% and 86% for 2H and 3R bilayers, respectively. Furthermore, we can reject nonphysical fits to indirect emission from monolayer regions by looking to the values of the fitted peak center (Fig. S8). If we directly map the I peak center, the difference between the 2H and 3R stacked bilayers is even clearer [Fig. 4(e)].

While we show that hyperspectral PL mapping is capable of distinguishing between different bilayer stacking, this comes at the cost of significantly longer measurement times. The collection time of the $355 \times 355\ \mu m^2$ SHG map in Fig. 3(a) was 3 min, the PL map shown in Fig. 3(a) took 40 min for a $7 \times 7\ \mu m^2$ scan (we note that the pixel width for the PL maps was 0.07 μm, whereas for SHG maps it was 0.13 μm). Although comparatively fast, bright-field, white-light imaging shows no contrast between stacking sequences, nor does AFM, which has a measurement time several orders of magnitude longer (Fig. 5).

In conclusion, we have demonstrated SHG microscopy as a powerful tool for assessing the size, distribution, and stacking order of bilayer nucleates in MOCVD-grown MoS_2 films. By correlating images taken by a variety of techniques, white-light microscopy, AFM, PL, and SHG, we unambiguously assign dark and bright islands seen in SHG images to 2H and 3R stacking orientations of bilayer nucleates on a crystallographically aligned MoS_2 monolayer film. We show that the imaging speed of SHG microscopy is a particular advantage when compared to other lab-scale techniques. We expect SHG microscopy to gain an important place as a tool to assess the prevalence and size dispersion of bi-, tri-, and multilayer nucleation in MOCVD films, giving further insight into their nucleation dynamics and the favorability toward growth of aligned and unaligned layers. Further studies of the method will push the development of SHG imaging for semiconductor metrology to detect other properties of TMD films grown by MOCVD at wafer scale, including defectivity, grain size, and strain by exploiting the polarization and pump wavelength dependence of the SHG response. It will also be of value to improve the imaging resolution through the generation of higher harmonics and using computational and optical techniques developed for this purpose.[43] Considerations must also be given to laser and detector requirements, as well as their compatibility with existing metrology tools and device stacks.[44] Our results pave the way for SHG microscopy to emerge as a powerful tool for the characterization of MOCVD-grown TMD films as advancements in synthesis require new measurement techniques.

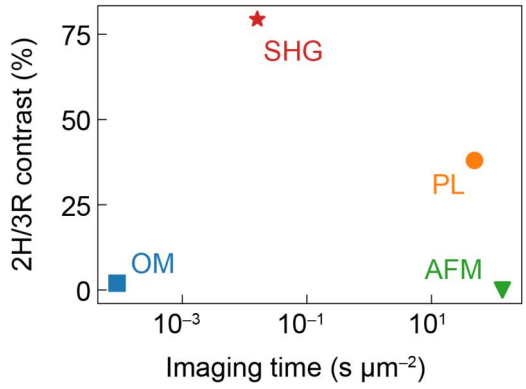

FIG. 5. Plot showing imaging time vs image contrast between 2H and 3R stacked bilayers for the methods used in this study: SHG, AFM, PL, and conventional bright-field, white-light microscopy (OM).

See the supplementary material for Secs. I–V, which contain experimental details of microscopy techniques, data analysis, and synthesis procedures. Figures S1–S7 show further optical images, histograms of bilayer island sizes, additional AFM data, microscopy of a trilayer island, example PL fits, and additional hyperspectral PL maps.

The authors wish to thank Roy van der Linden for assistance with autocorrelation measurements and Falco Bijloo and Masha Ogienko for helpful discussions. This work has been carried out at the Advanced Research Center for Nanolithography (ARCNL), a public–private partnership between the University of Amsterdam (UvA), the Vrije Universiteit Amsterdam (VU), the Rijksuniversiteit Groningen (RUG), the Netherlands Organization for Scientific Research (NWO), and the semiconductor-equipment manufacturer ASML. This work was (partly) financed by 'Toeslag voor Topconsortia voor Kennis en Innovatie (TKI)' from the Dutch Ministry of Economic Affairs and Climate.

AUTHOR DECLARATIONS

Conflict of Interest

The authors have no conflicts to disclose.

Author Contributions

Reynolds Dziobek-Garrett: Conceptualization (equal); Investigation (equal); Methodology (equal); Resources (equal); Visualization (equal); Writing – original draft (equal); Writing – review & editing (equal). **Vina Faramarzi:** Conceptualization (equal); Methodology (equal); Project administration (equal); Resources (equal); Supervision (equal); Writing – original draft (equal); Writing – review & editing (equal). **Pawan Kumar:** Conceptualization (equal); Investigation (equal); Methodology (equal); Resources (equal); Writing – original draft (equal); Writing – review & editing (equal). **Vasco Tenner:** Conceptualization (equal); Investigation (equal); Methodology (equal); Writing – review & editing (equal). **Marko Kamp:** Conceptualization (equal); Funding acquisition (equal); Investigation (equal); Methodology (equal); Project administration (equal); Resources (equal); Supervision (equal); Writing – original draft (equal); Writing – review & editing (equal). **A. Femius Koenderink:** Conceptualization (equal); Funding acquisition (equal); Methodology (equal); Project administration (equal); Resources (equal); Supervision (equal); Writing – original draft (equal); Writing – review & editing (equal). **Jorik van de Groep:** Conceptualization (equal); Funding acquisition (equal); Methodology (equal); Project administration (equal); Supervision (equal); Writing – original draft (equal);

Writing – review & editing (equal). **Roland Bliem:** Conceptualization (equal); Funding acquisition (equal); Methodology (equal); Project administration (equal); Supervision (equal); Writing – original draft (equal); Writing – review & editing (equal).

DATA AVAILABILITY

The data that support the findings of this study are available from the corresponding author upon reasonable request.

REFERENCES

[1]Y. Liu, X. Duan, H.-J. Shin, S. Park, Y. Huang, and X. Duan, "Promises and prospects of two-dimensional transistors," Nature **591**, 43–53 (2021).

[2]S. A. Iyengar, S. Bhattacharyya, S. Roy, N. R. Glavin, A. K. Roy, and P. M. Ajayan, "A researcher's perspective on unconventional lab-to-fab for 2D semiconductor devices," ACS Nano **17**, 12955–12970 (2023).

[3]M. Mattinen, M. Leskelä, and M. Ritala, "Atomic layer deposition of 2D metal dichalcogenides for electronics, catalysis, energy storage, and beyond," Adv. Mater. Interfaces **8**, 2001677 (2021).

[4]L. Sun, G. Yuan, L. Gao, J. Yang, M. Chhowalla, M. H. Gharahcheshmeh, K. K. Gleason, Y. S. Choi, B. H. Hong, and Z. Liu, "Chemical vapour deposition," Nat. Rev. Methods Primers **1**, 5 (2021).

[5]T. H. Choudhury, X. Zhang, Z. Y. Balushi, M. Chubarov, and J. M. Redwing, "Epitaxial growth of two-dimensional layered transition metal dichalcogenides," Annu. Rev. Mater. Res. **50**, 155–177 (2020).

[6]T. Chowdhury, E. C. Sadler, and T. J. Kempa, "Progress and prospects in transition-metal dichalcogenide research beyond 2D," Chem. Rev. **120**, 12563–12591 (2020).

[7]R. Dziobek-Garrett, S. Hilliard, S. Sriramineni, O. Ambrozaite, Y. Zhu, B. M. Hudak, T. H. Brintlinger, T. Chowdhury, and T. J. Kempa, "Controlling morphology and excitonic disorder in monolayer WSe_2 grown by salt-assisted CVD methods," ACS Nanosci. Au **3**, 441–450 (2023).

[8]T. Zhang, J. Wang, P. Wu, A.-Y. Lu, and J. Kong, "Vapour-phase deposition of two-dimensional layered chalcogenides," Nat. Rev. Mater. **8**, 799–821 (2023).

[9]Z. Qin, L. Loh, J. Wang, X. Xu, Q. Zhang, B. Haas, C. Alvarez, H. Okuno, J. Z. Yong, T. Schultz, N. Koch, J. Dan, S. J. Pennycook, D. Zeng, M. Bosman, and G. Eda, "Growth of Nb-doped monolayer WS_2 by liquid-phase precursor mixing," ACS Nano **13**, 10768–10775 (2019).

[10]H. Li, Y. Li, A. Aljarb, Y. Shi, and L. J. Li, "Epitaxial growth of two-dimensional layered transition-metal dichalcogenides: Growth mechanism, controllability, and scalability," Chem. Rev. **118**, 6134–6150 (2018).

[11]T. Li, W. Guo, L. Ma, W. Li, Z. Yu, Z. Han, S. Gao, L. Liu, D. Fan, Z. Wang, Y. Yang, W. Lin, Z. Luo, X. Chen, N. Dai, X. Tu, D. Pan, Y. Yao, P. Wang, Y. Nie, J. Wang, Y. Shi, and X. Wang, "Epitaxial growth of wafer-scale molybdenum disulfide semiconductor single crystals on sapphire," Nat. Nanotechnol. **16**, 1201–1207 (2021).

[12]L. Zhang, J. Dong, and F. Ding, "Strategies, status, and challenges in wafer scale single crystalline two-dimensional materials synthesis," Chem. Rev. **121**, 6321–6372 (2021).

[13]H. Zhu, N. Nayir, T. H. Choudhury, A. Bansal, B. Huet, K. Zhang, A. A. Puretzky, S. Bachu, K. York, T. V. Knight, N. Trainor, A. Oberoi, K. Wang, S. Das, R. A. Makin, S. M. Durbin, S. Huang, N. Alem, V. H. Crespi, A. C. van Duin, and J. M. Redwing, "Step engineering for nucleation and domain orientation control in WSe_2 epitaxy on c-plane sapphire," Nat. Nanotechnol. **18**, 1295–1302 (2023).

[14]H. Yu, L. Huang, L. Zhou, Y. Peng, X. Li, P. Yin, J. Zhao, M. Zhu, S. Wang, J. Liu, H. Du, J. Tang, S. Zhang, Y. Zhou, N. Lu, K. Liu, N. Li, and G. Zhang, "Eight in. wafer-scale epitaxial monolayer MoS_2," Adv. Mater. **36**, 2402855 (2024).

[15]M. Georgieva, N. Petkov, and R. Duffy, "3D to 2D perspectives—Traditional and new doping and metrology challenges at the nanoscale," Mater. Sci. Semicond. Process. **163**, 107584 (2023).

[16]U. Celano, D. Schmidt, C. Beitia, G. Orji, A. V. Davydov, and Y. Obeng, "Metrology for 2D materials: Perspective review from the international roadmap for devices and systems," Nanoscale Adv. **6**, 2260–2269 (2024).

[17]L. M. Malard, T. V. Alencar, A. P. M. Barboza, K. F. Mak, and A. M. de Paula, "Observation of intense second harmonic generation from MoS_2 atomic crystals," Phys. Rev. B **87**, 201401 (2013).

[18]Y. Li, Y. Rao, K. F. Mak, Y. You, S. Wang, C. R. Dean, and T. F. Heinz, "Probing symmetry properties of few-layer MoS_2 and H-BN by optical second-harmonic generation," Nano Lett. **13**, 3329–3333 (2013).

[19]W.-T. Hsu, Z.-A. Zhao, L.-J. Li, C.-H. Chen, M.-H. Chiu, P.-S. Chang, Y.-C. Chou, and W.-H. Chang, "Second harmonic generation from artificially stacked transition metal dichalcogenide twisted bilayers," ACS Nano **8**, 2951–2958 (2014).

[20]S. M. Shinde, K. P. Dhakal, X. Chen, W. S. Yun, J. Lee, H. Kim, and J. H. Ahn, "Stacking-controllable interlayer coupling and symmetric configuration of multilayered MoS_2," NPG Asia Mater. **10**, e468 (2018).

[21]L. Mennel, M. Paur, and T. Mueller, "Second harmonic generation in strained transition metal dichalcogenide monolayers: MoS_2, $MoSe_2$, WS_2, and WSe_2," APL Photonics **4**, 34404 (2019).

[22]X. Yin, Z. Ye, D. A. Chenet, Y. Ye, K. O'Brien, J. C. Hone, and X. Zhang, "Edge nonlinear optics on a MoS_2 atomic monolayer," Science **344**, 488–490 (2014).

[23]L. Karvonen, A. Säynätjoki, M. J. Huttunen, A. Autere, B. Amirsolaimani, S. Li, R. A. Norwood, N. Peyghambarian, H. Lipsanen, G. Eda, K. Kieu, and Z. Sun, "Rapid visualization of grain boundaries in monolayer MoS_2 by multiphoton microscopy," Nat. Commun. **8**, 15714 (2017).

[24]L. Liu, T. Li, X. Gong, H. Wen, L. Zhou, M. Feng, H. Zhang, N. Zou, S. Wu, Y. Li, S. Zhu, F. Zhuo, X. Zou, Z. Hu, Z. Ding, S. Fang, W. Xu, X. Hou, K. Zhang, G. Long, L. Tang, Y. Jiang, Z. Yu, L. Ma, J. Wang, and X. Wang, "Homoepitaxial growth of large-area rhombohedral-stacked MoS_2," Nat. Mater. **24**, 1195–1202 (2025).

[25]T. Schram, Q. Smets, A. Opdebeeck, S. Ghosh, B. Groven, P. Kumar, H. M. Medina, D. Cott, J.-F. deMarneffe, H. Dongre, A. Kruv, L. Panarella, L. F. Pinotti, P. Morin, G. S. Kar, and C. J. L. de la Rosa, "Integration and electrical evaluation of WS_2 and MoS_2 FETs in a 300 mm pilot line," Discover Electron. **3**, 15 (2026).

[26]T. S. Kim, G. Noh, S. Kwon, J. Y. Kim, K. P. Dhakal, S. Oh, H. J. Chai, E. Park, I. S. Kim, E. Lee, Y. Kim, J. Lee, M. kyung Jo, M. Kang, C. Park, J. Kim, J. Park, S. Kim, M. Kim, Y. Kim, S. Y. Choi, S. Song, H. Y. Jeong, J. Kim, J. Y. Kwak, and K. Kang, "Diffusion control on the van der Waals surface of monolayers for uniform bi-layer MoS_2 growth," Adv. Funct. Mater. **34**, 2312365 (2024).

[27]T. S. Kim, K. P. Dhakal, E. Park, G. Noh, H.-J. Chai, Y. Kim, S. Oh, M. Kang, J. Park, J. Kim, S. Kim, Y. Jeong, S. Bang, J. Y. Kwak, J. Kim, K. Kang, T. S. Kim, G. Noh, H.-J. Chai, S. Oh, M. Kang, J. Park, J. Kim, S. Kim, K. Kang, K. P. Dhakal, Y. Kim, E. Park, J. Y. Kwak, H. Y. Jeong, and S. Bang, "Gas-phase alkali metal-assisted MOCVD growth of 2D transition metal dichalcogenides for large-scale precise nucleation control," Small **18**, 2106368 (2022).

[28]I. Kandybka, B. Groven, H. M. Silva, S. Sergeant, A. N. Mehta, S. Koylan, Y. Shi, S. Banerjee, P. Morin, and A. Delabie, "Chemical vapor deposition of a single-crystalline MoS_2 monolayer through anisotropic 2D crystal growth on stepped sapphire surface," ACS Nano **18**, 3173–3186 (2024).

[29]J. Verdin, H. M. Silva, A. N. Mehta, I. Kandybka, B. Groven, P. Kumar, S. Koylan, S. Sergeant, P. Favia, P. Morin, and A. Delabie, "Process-induced modulation of domain orientations during WS_2 epitaxy by metal-organic chemical vapor deposition on sapphire," ACS Appl. Electron. Mater. **6**, 6758–6769 (2024).

[30]J. Shi, P. Yu, F. Liu, P. He, R. Wang, L. Qin, J. Zhou, X. Li, J. Zhou, X. Sui, S. Zhang, Y. Zhang, Q. Zhang, T. C. Sum, X. Qiu, Z. Liu, and X. Liu, "3R MoS_2 with broken inversion symmetry: A promising ultrathin nonlinear optical device," Adv. Mater. **29**, 1701486 (2017).

[31]D. Yang, J. Liang, J. Wu, Y. Xiao, J. I. Dadap, K. Watanabe, T. Taniguchi, and Z. Ye, "Non-volatile electrical polarization switching via domain wall release in 3R-MoS_2 bilayer," Nat. Commun. **15**, 1389 (2024).

[32]X. Li, X. Shi, D. Marian, D. Soriano, T. Cusati, G. Iannaccone, G. Fiori, Q. Guo, W. Zhao, and Y. Wu, "Rhombohedral-stacked bilayer transition metal dichalcogenides for high-performance atomically thin CMOS devices," Sci. Adv. **9**, eade5706 (2023).

[33]J. Strachan, A. F. Masters, and T. Maschmeyer, "3R-MoS_2 in review: History, status, and outlook," ACS Appl. Energy Mater. **4**, 7405–7418 (2021).

[34]J. He, K. Hummer, and C. Franchini, "Stacking effects on the electronic and optical properties of bilayer transition metal dichalcogenides MoS_2, $MoSe_2$, WS_2, and WSe_2," Phys. Rev. B **89**, 075409 (2014).
[35]A. N. Mehta, N. Gauquelin, M. Nord, A. Orekhov, H. Bender, D. Cerbu, J. Verbeeck, and W. Vandervorst, "Unravelling stacking order in epitaxial bilayer MX_2 using 4D-STEM with unsupervised learning," Nanotechnology **31**, 445702 (2020).
[36]L. Liu, T. Li, L. Ma, W. Li, S. Gao, W. Sun, R. Dong, X. Zou, D. Fan, L. Shao, C. Gu, N. Dai, Z. Yu, X. Chen, X. Tu, Y. Nie, P. Wang, J. Wang, Y. Shi, and X. Wang, "Uniform nucleation and epitaxy of bilayer molybdenum disulfide on sapphire," Nature **605**, 69–75 (2022).
[37]P. D. Hanrahan, R. Dziobek-Garrett, P. M. Eckhert, C. Leiter, K. Kingsbury, K. Davydov, L. Gu, T. H. Brintlinger, S. B. Ambade, Y. Zhou, and T. J. Kempa, "Improved grain growth in large-area monolayer WX_2 (X: S, Se) films through controlled reduction of tungstate precursors," Chem. Mater. **38**, 6227–6236 (2026).
[38]R. Akashi, M. Ochi, S. Bordács, R. Suzuki, Y. Tokura, Y. Iwasa, and R. Arita, "Two-dimensional valley electrons and excitons in noncentrosymmetric 3R-MoS_2," Phys. Rev. Appl. **4**, 014002 (2015).
[39]I. Paradisanos, S. Shree, A. George, N. Leisgang, C. Robert, K. Watanabe, T. Taniguchi, R. J. Warburton, A. Turchanin, X. Marie, I. C. Gerber, and B. Urbaszek, "Controlling interlayer excitons in MoS_2 layers grown by chemical vapor deposition," Nat. Commun. **11**, 2391 (2020).
[40]S. Anghel, Y. Chumakov, V. Kravtsov, G. Volodina, A. Mitioglu, P. Plochocka, K. Sushkevich, E. Mishina, and L. Kulyuk, "Site-selective luminescence spectroscopy of bound excitons and local band structure of chlorine intercalated 2H- and 3R-MoS_2 polytypes," J. Lumin. **177**, 331–336 (2016).
[41]R. Suzuki, M. Sakano, Y. J. Zhang, R. Akashi, D. Morikawa, A. Harasawa, K. Yaji, K. Kuroda, K. Miyamoto, T. Okuda, K. Ishizaka, R. Arita, and Y. Iwasa, "Valley-dependent spin polarization in bulk MoS_2 with broken inversion symmetry," Nat. Nanotechnol. **9**, 611–617 (2014).
[42]J. V. Baren, G. Ye, J. A. Yan, Z. Ye, P. Rezaie, P. Yu, Z. Liu, R. He, and C. H. Lui, "Stacking-dependent interlayer phonons in 3R and 2H MoS_2," 2D Mater. **6**, 025022 (2019).
[43]K. Murzyn, M. L. van der Geest, L. Guery, Z. Nie, P. van Essen, S. Witte, and P. M. Kraus, "Breaking Abbe's diffraction limit with harmonic deactivation microscopy," Sci. Adv. **10**, eadp2056 (2024).
[44]E. Abram, R. Dziobek-Garrett, V. Faramarzi, R. Bliem, and P. Planken, "Light-induced damage in semiconductor device manufacturing: Present and future challenges," J. Appl. Phys. **139**, 80901 (2026).